Classical decoherence in a nanomechanical resonator

Olivier Maillet, Frantisek Vavrek, Andrew D. Fefferman, Olivier Bourgeois, Eddy Collin

Classical decoherence in a nanomechanical resonator

Olivier Maillet[1], František Vavrek[2], Andrew D. Fefferman[1], Olivier Bourgeois[1] & Eddy Collin[1]

[1] *Institut Néel, CNRS and Université Grenoble Alpes, F-38042 Grenoble, France*
[2] *Centre of Low Temperature Physics, Institute of Experimental Physics, S. A. S. and P. J. Šafárik University Košice, Watsonova 47, 04001 Košice, Slovakia*

Decoherence is an essential mechanism that defines the boundary between classical and quantum behaviours, while imposing technological bounds for quantum devices. Little is known about quantum coherence of mechanical systems, as opposed to electromagnetic degrees of freedom. But decoherence can also be thought of in a purely classical context, as the loss of phase coherence in the classical phase space. Indeed the bridge between quantum and classical physics is under intense investigation, using classical nanomechanical analogues of quantum phenomena. In the present work, by separating pure dephasing from dissipation, we quantitatively model the classical decoherence of a mechanical resonator: through the experimental control of frequency fluctuations, we engineer artificial dephasing. We report on the methods to define pure dephasing in these systems, which are prerequisite in the understanding of decoherence processes in mechanical devices, both classical and quantum.

Corresponding Author: E.C. (eddy.collin@neel.cnrs.fr)

Decoherence can be viewed either in its quantum picture, where it stands for the loss of phase coherence of a superposition state [1, 2], or as its classical equivalent, where the phase of an oscillating signal is smeared due to frequency fluctuations [3]. Until recently, dissipation, which accounts for an energy loss over time [4], was not distinguished from decoherence in nanomechanical resonators. The first reason for this oversight lies in the acquisition method: spectral acquisition, in which the driving frequency is swept through the mechanical resonance, does not separate the two processes, since both lead to broadened resonance lines. The response linewidth then leads to the definition of a decoherence time T_2, in analogy with nuclear magnetic resonance (NMR) [5] or quantum information experiments [6, 7]. One way to unravel a dephasing mechanism is to perform a complementary time-domain ringdown measurement. Here, the free decay of the response amplitude yields an energy relaxation time, since the decay rate only depends on dissipation, not frequency fluctuations. This procedure is analogous to a T_1 measurement for spins or qubits. Having $T_1 \neq T_2$ then leads to the definition of a pure dephasing rate Γ_ϕ [6].

While the reported T_1 and T_2 for a particular qubit are often significantly different [7], such a difference in a nanomechanical resonator is still rare in the literature: usually mechanical systems seem to experience frequency fluctuations small compared to dissipation mechanisms, and do not exhibit visible spectral broadening due to dephasing [8–11]. Thus, the second and main reason for the scarcity of experimental studies on mechanical decoherence is a lack of very precise measurements, performed over a vast domain of devices and dynamic ranges. To our knowledge, only one recent study reports, for a suspended carbon nanotube, a signature of a pure (yet nonlinear) dephasing mechanism [6], while another study presents similar features interpreted as nonlinear damping [12]. Nonetheless the effects of frequency noise (and its origin) in nanomechanical devices is a subject intensely investigated today, both for its fundamental aspects and the technical limitations it poses to actual devices [13–21]. Besides, with the advances of quantum nanomechanics, the decoherence of quantum mechanical states also becomes a challenging issue [8, 22, 23].

In this article we report on a model experiment using a high quality nanoelectromechanical system (NEMS), top-down fabricated from high-stress silicon-nitride (SiN) [4, 16]. Using a gate electrode [24], we capacitively control the oscillator's frequency fluctuations by applying voltage noise, leading to a completely quantitative description of mechanical decoherence. First we perform time and frequency domain measurements without noise applied on the gate, in order to ensure that no pure dephasing is observed over our whole dynamic range, from linear to highly nonlinear regimes: we thus establish our device as ideal for our study. In a second part, a low-frequency noise gate voltage is injected, leading to resonance frequency fluctuations increasing with the noise level: indeed, a significant spectral broadening is observed, while ringdown measurements leave T_1 unchanged, demonstrating pure dephasing with $T_1 \neq T_2$. We present the complete formalism applying to low-frequency fluctuations of the resonance frequency. Building on the new methods presented, we furthermore discuss the possibility to extract information about the fluctuations statistics from the shape of the spectral response in actual devices suffering from dephasing.

Results

The nanoelectromechanical system.

Fig. 1b) shows a scanning electron microscope picture of the measured NEMS. This device consists in a 295 μm long x 100 nm thick x 300 nm wide doubly-clamped high-stress silicon nitride (Si_3N_4) suspended beam, with a 90 nm thick conducting aluminium layer on top. A gate electrode is made in the vicinity of the beam, separated by a gap $g \approx 3$ μm, over a 250 μm length. The total mass of the device is $M = 4.7 \times 10^{-14}$ kg. The experiment is performed at 4.2 K in a cryogenic vacuum (pressure $< 10^{-6}$ mbar).

We first perform a careful calibration of the whole setup following Ref. [25], giving access to displacements and injected driving force in real units. Fig. 1a) shows the schematic of the experimental setup. A drive voltage is applied through a 1 kΩ bias resistor, injecting a current in the aluminium layer of the NEMS. Actuation and detection follow the magnetomotive scheme [25, 26], with a magnetic field $B < 1$ T. The voltage induced by the motion is measured by standard lock-in detection with its in-phase (X) and quadrature (Y) components.

We work on the fundamental flexural mode $n = 0$, having effective spring constant k_0, mass m_0 and applied sinusoidal force amplitude F_0. The typical response to a sinusoidal driving force in the linear regime is displayed in Fig. 1c). The resonance frequency is measured at $\omega_0 = 2\pi \times 0.66$ MHz, which is in good agreement with calculated properties. In the following, in order to min-

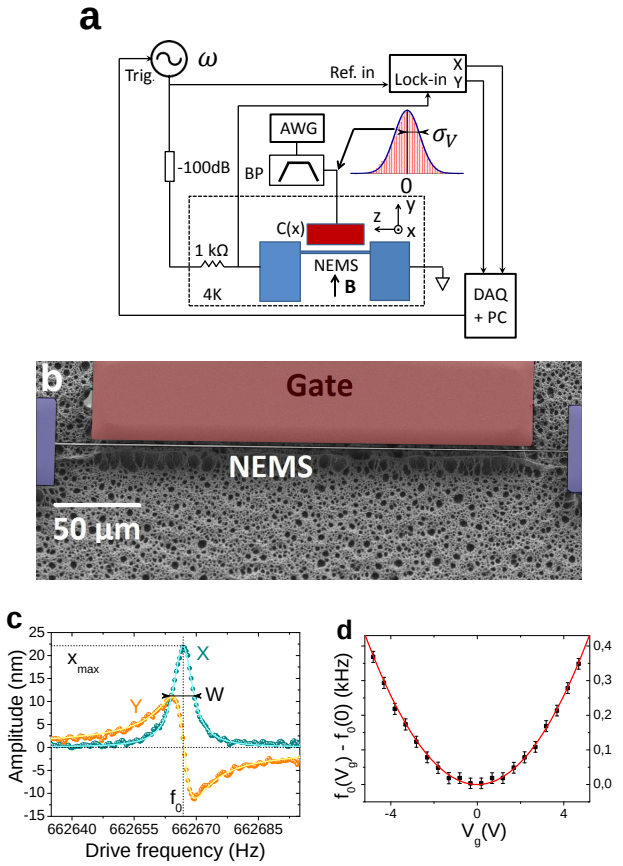

Figure 1: **Experimental setup and device characterization. (a)** Schematic view of the measurement setup. A sinusoidal current is fed into the cryogenic NEMS, actuated and detected through the magnetomotive technique. The detected signal is processed with a lock-in amplifier. An arbitrary waveform generator delivers the gate voltage. The bandpass filter is used only when the injected voltage is a Gaussian noise (typical histogram shown, with fit leading to $\sigma_V = 490$ mV). **(b)** Coloured SEM picture of the nanomechanical oscillator capacitively coupled to a gate electrode. **(c)** Standard linear response to a sinusoidal driving force of amplitude $F_0 = 83$ fN, with its in-phase X(ω) and quadrature Y(ω) components. Solid lines correspond to a (complex) Lorentzian line shape fit, with full width at half maximum (FWHM) W, position $f_0 = \omega_0/(2\pi)$ and height x_{max}. **(d)** Shift of the NEMS resonance frequency f_0 as a DC voltage is applied to the gate electrode. The red solid line is a parabolic fit with a coefficient $\alpha/(2\pi)$.

imize electrical losses [27], we keep a low magnetic field $B = 0.1$ T. The damping rate is then $\Delta\omega_0 = 2\pi \times 5.6$ Hz, hence a quality factor $Q \approx 118\,000$. Here $Q \gg 1$ so we can write the susceptibility in the standard Lorentzian approximation: $\chi_0(\omega) = [2m_0\omega_0(\omega_0 - \omega - i\Delta\omega_0/2)]^{-1}$. In our notations, we define in-phase $\mathrm{X}(\omega) = \mathrm{Im}[\chi_0(\omega)]F_0$ and quadrature $\mathrm{Y}(\omega) = \mathrm{Re}[\chi_0(\omega)]F_0$ components of the motion.

A DC voltage V_g is then delivered with an arbitrary waveform generator (AWG) on the gate electrode, which forms a geometric capacitance $C(x)$ with the beam itself. The energy stored by the capacitor can be written as $E_C = C(x)V_g^2/2$. Thus the additional electrostatic force acting on the beam along the x axis is $F_C = (V_g^2/2)\partial C(x)/\partial x$. Expanding F_C in a Taylor series [24, 25], we obtain the effect of the DC voltage on the resonance through a frequency pulling term:

$$\omega_0(V_g) - \omega_0(0) \approx -\frac{1}{4m_0\omega_0}\frac{\partial^2 C(0)}{\partial x^2}V_g^2 = \alpha V_g^2 \qquad (1)$$

Here $\partial^2 C(0)/\partial x^2$ is defined as the coupling strength, and $\alpha > 0$ is a constant only determined by the oscillator's intrinsic quantities and the coupling strength. We measure $\alpha = 2\pi \times 16.44$ Hz/V^2 [see Fig. 1 d)], hence a coupling strength $\partial^2 C(0)/\partial x^2 = -4.3 \times 10^{-5}$ F/m^2 (more details on the magnetomotive scheme, setup and capacitive coupling can be found in supplementary material [28]).

Absence of nonlinear dephasing and relaxation.

When driven with high input forces, our NEMS' oscillation amplitude at resonance becomes high enough so its dynamics enters the so-called "Duffing" regime, arising from a geometric non-linearity: the tensioning effect. The frequency domain response bends toward higher frequency and the resonance is shifted quadratically with the motion, eventually leading to a bistable regime [29, 30]. In doubly-clamped SiN nano-beams this non-linearity is known to be important [31], which means that already modest drive excitations can bring the device into the Duffing regime. This fact naturally brings in two questions: are there as well any nonlinear relaxation/decoherence processes to discover in SiN structures, like for nanotubes [6, 12] ? And how do we perform T_1 and T_2 measurements within a highly nonlinear/bistable dynamic system ?

In the following we describe how to measure T_1 and T_2 response times that we defined in analogy with NMR over the whole dynamic range, in order to compare them as a function of motion amplitude. The relaxation time T_1 obtained from ringdown measurements is only sensitive to dissipation mechanisms, by analogy with longitudinal relaxation time in the Bloch sphere for two-level

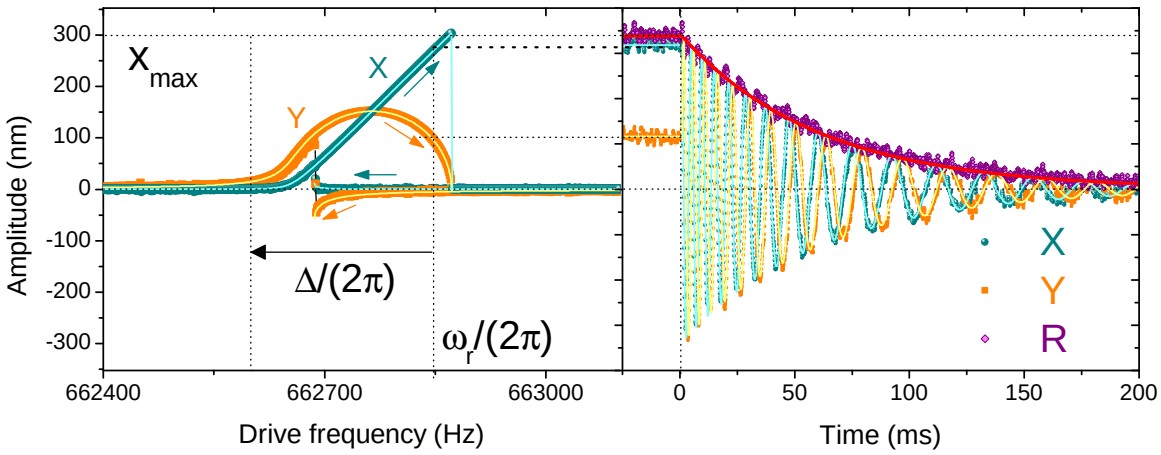

Figure 2: **Nonlinear response.** Frequency and time domain response of the mechanical oscillator, in X and Y quadratures. The applied sinusoidal driving force of amplitude $F_0 = 1.1$ pN enables the resonator to reach the bistable regime. The two branches of the hysteretic response are displayed in the frequency domain on the left panel (see arrows for the frequency sweep direction). The free decay of the steady state response (right panel) is measured after detuning the drive from the resonance ω_r by $\Delta = -2\pi \times 250$ Hz. Solid lines are theoretical fits from the Duffing oscillator model (left) and the Lindstedt-Poincaré method (right). The magenta curve on the right panel corresponds to the amplitude $\mathrm{R} = \sqrt{\mathrm{X}^2 + \mathrm{Y}^2}$, fit to an exponential decay of time constant T_1 (full curve).

systems. The ringdown is triggered by exciting the device at large motion amplitude at frequency ω_r close to ω_0, and suddenly detuning the driving force to a frequency $\omega_r + \Delta$ where the device is off resonance. The beating of the mechanics with the local oscillator is then recorded [32] (see Fig. 2 right panel). To obtain the plots, about $N \simeq 100$ to 1000 decays have been averaged. The T_2 time is obtained from frequency sweeps across the resonance, with each point averaged over a time long enough to make sure that we are sensitive to potential low-frequency fluctuations (see Fig. 2 left panel). T_2 is affected both by dissipation and phase fluctuations, in a similar manner to the transverse relaxation time in NMR or qubit measurements. But one fundamental difference is that here we are dealing with an almost harmonic classical oscillator, not a quantum two-level system, so the analogy is restricted to the phenomenology of the decoherence phenomenon. Moreover, while for qubits and spins the pure dephasing Γ_ϕ is defined through the comparison between T_2 and $2T_1$ [7], in our system T_2 has to be compared to T_1, similarly to the case of a classical spin [10].

Fig. 2 shows both frequency and time-domain measurements in a highly nonlinear regime, with a peak-to-peak maximum amplitude of about 600 nm, that is, more than three times the NEMS thickness. Here the bistable resonance line can be fit according to the Duffing model for nonlinear oscillators [32]. In the linear regime, the FWHM W of the X quadrature directly yields the Lorentzian parameter $\Delta\omega_0/(2\pi)$ and is used to define $T_2 = (\pi W)^{-1}$. In the strongly nonlinear case, from the measured maximum amplitude x_{max} one can calculate [32] the intrinsic linewidth parameter $\Delta\omega_0$ used for the full nonlinear fit: $\Delta\omega_0 = F_0/(m_0\omega_0 x_{max})$. This parameter can again be converted into a T_2. The latter is displayed as a function of motion amplitude in Fig. 3 (blue dots). The time-decay oscillation can be fit using the Lindstedt-Poincaré method [32]. The relaxation is found to be exponential over the entire range studied, leading to a T_1 showed in Fig. 3 (red dots). The ringdown measurement yields a relaxation time $T_1 \simeq 58$ ms $\pm$ 3 ms in the whole attainable amplitude range, which matches the T_2 time of spectral data defined as $2/\Delta\omega_0 \simeq 57$ ms $\pm$ 3 ms: we thus verify

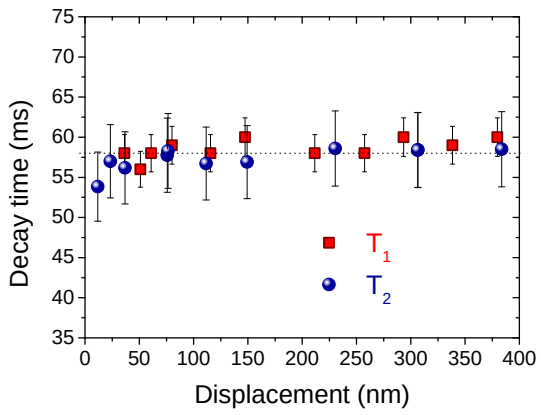

Figure 3: **Decay times in nonlinear regime.** Relaxation (T_1) and decoherence (T_2) times as a function of motion amplitude. The dotted line is set at 58 ms.

$T_1 = T_2$ within $\pm$ 8 %. In other words, we do not identify any sources of nonlinear damping or dephasing in our SiN system, as opposed to carbon-based devices [6, 12]. This result is achieved over an unprecendently broad dynamic range, with a measurement technique that can be adapted to other devices, in particular graphene or nanotube ones. As far as the present work is concerned, this establishes our device as an ideal NEMS resonator.

Controlling pure dephasing.

In order to introduce a dephasing process, we deliver a Gaussian noise with the AWG connected to the gate electrode, instead of the DC voltage used previously for calibration purposes. Our aim is to model "slow" fluctuations of the resonance frequency, that is with correlation times longer than the relaxation time T_1 [18]. In the aforementioned work, the interplay of the driving force with the frequency noise spectrum is characterized, in order to separate fast and slow noise contributions. Complementarily, we focus here on how the driven response evolves with respect to the level of slow fluctuations. Furthermore, in Ref. [18], the frequency noise is experimentally taken to be Gaussian; we on the other hand extend the study to highly asymmetric statistics.

To keep only low-frequency fluctuations while avoiding spurious $1/f$ noise coming from the setup, the delivered voltage noise is thus filtered [see Fig. 1a)] below 40 mHz and above 0.8 Hz (-3 dB cut-off frequencies). The resulting voltage fluctuations on the gate electrode, represented by the Gaussian random variable δV_g, of mean value 0 and root mean square value $\sigma_V = \langle \delta V_g^2 \rangle^{1/2}$, translate through the capacitive coupling into fluctuations of the resonance frequency. Following Eq. (1) the new random variable associated with these fluctuations is $\delta\Omega(t) = \alpha \delta V_g^2(t)$, with a probability distribution defined over positive frequencies [see Fig. 4b) inset]:

$$\rho_\sigma(\delta\Omega) = \left(\frac{1}{\sqrt{2}\pi\sigma\delta\Omega}\right)^{1/2} \exp\left(-\frac{\delta\Omega}{\sqrt{2}\sigma}\right) \qquad (2)$$

where $\sigma = \sqrt{2}\alpha\sigma_V^2 = [\langle\delta\Omega^2\rangle - \langle\delta\Omega\rangle^2]^{1/2}$ is the standard deviation of the distribution, taken as a characteristic frequency noise level (in rad.s^{-1}). This is the effective tunable parameter with which we characterize decoherence in our system. Mathematically, we show that the averaging of fluctuations can be treated similarly to the case of "inhomogeneous broadening" in NMR [5], spatial-disorder being replaced, as for qubits, by time-dependent disorder (see supplementary information [28]). Knowing the distribution ρ_σ, the altered susceptibility can thus be written as the convolution of the mechanical response χ_0 in the high Q Lorentzian limit by the distribution ρ_σ:

$$\chi_\sigma(\omega) = \int_0^{+\infty} \chi_0(\omega - \delta\Omega)\rho_\sigma(\delta\Omega)\mathrm{d}\delta\Omega \qquad (3)$$

Note that σ is also defined through $S_\Omega(\omega)$, the spectrum of the frequency fluctuations, with $\langle\delta\Omega^2\rangle = (2\pi)^{-1}\int S_\Omega(\omega)\mathrm{d}\omega = 3\sigma^2/2$. Thus Eq. (3) is valid only if the noise power is integrable (which justifies mathematically the introduction of a higher cut-off frequency). In particular for $1/f$ noise, dephasing would depend on the measurement time since the lower bound of the spectrum would be fixed by the experiment duration itself (which justifies our lower cut-off filtering choice).

Fig. 4 shows frequency domain measurements for different noise levels, with theoretical calculations without free parameters from Eq. (3), clearly showing spectral broadening. The convolution picture provides a rather intuitive interpretation: while the noise level σ responsible for pure dephasing is kept small enough compared to the mechanical damping rate $\Delta\omega_0$, one can approximate the distribution ρ_σ as a Dirac delta function, and then the convolution leaves the Lorentzian susceptibility unchanged. When σ becomes comparable to the damping rate, the distribution leaves its imprint in the mechanical response, as an evidence for mechanical dephasing: here, the resonance line is asymmetrically broadened, which is a signature for the non-Gaussian nature of the fluctuations (see discussion below). For large fluctuations

($\sigma \gg \Delta\omega_0$) a significant deviation from the Lorentzian lineshape is observed (see discussion) and the resonance peak looks like the distribution ρ_σ itself, the initial susceptibility being almost a Delta function.

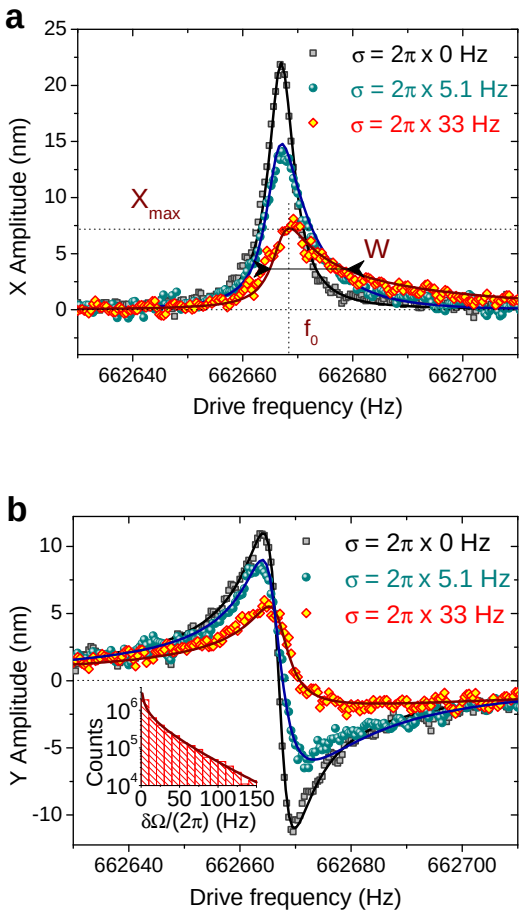

Figure 4: **Frequency response with engineered slow fluctuations.** Frequency sweep measurements in **(a)** phase (X) and **(b)** quadrature (Y) components of the mechanical response $x_\sigma(\omega) = \chi_\sigma(\omega)F_0$, with a sinusoidal driving force of amplitude $F_0 = 83$ fN. Solid lines are theoretical curves calculated from Eq. (3), and resonance line parameters W, f_0 are shown in a). Inset in **(b)**: frequency noise histogram at $\sigma = 2\pi\times 33$ Hz calculated from δV_g^2 measurements, for 4×10^6 counts. The solid line is the application of Eq. (2).

The time domain measurements (see Fig. 5) performed for different noise levels yield unambiguously the same decay time $T_1 \simeq 57$ ms $\simeq 1/(\pi \times 5.6$ Hz) within $\pm$ 5% for all data sets [see Fig. 5 and 6a)]. Interestingly, T_2 can also be measured via time-domain measurements, by averaging first X and Y quadratures over N relaxations, and then computing $\langle \mathrm{R}\rangle_N^2 = \langle \mathrm{X}\rangle_N^2 + \langle \mathrm{Y}\rangle_N^2$. Indeed the quadratures taken independently are sensitive to frequency fluctuations, while the direct measurement of $\langle \mathrm{R}^2\rangle_N = \langle \mathrm{X}^2 + \mathrm{Y}^2\rangle_N$ is not. The obtained curve (see Fig. 5) can be well fit with an exponential law, yielding a decay time in very good agreement with the T_2 defined from frequency domain measurements [see Fig. 6a)]. For simplicity we call this time domain measurement of decoherence $\overline{T}_2$.

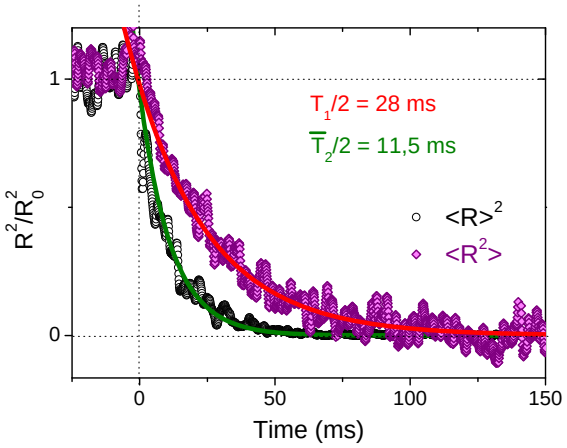

Figure 5: **Ringdown measurements under frequency fluctuations.** Time domain measurements of $\langle \mathrm{R}^2\rangle_N$ (magenta) and $\langle \mathrm{R}\rangle_N^2$ (black, empty dots), normalized to their steady state resonant amplitudes of motion $\langle \mathrm{R}_0^2\rangle_N$ and $\langle \mathrm{R}_0\rangle_N^2$. Solid lines are exponential fits. Data acquired for $\sigma = 2\pi \times 33$ Hz, $F_0 = 83$ fN.

For a quantitative discussion we plot in Fig. 6a) the $T_2 = (\pi W)^{-1}$ obtained from a simple estimate of the FWHM in the frequency domain [see Fig. 4a)], together with $\overline{T}_2$ and T_1. Starting at the initial value of $2/\Delta\omega_0 \approx 57$ ms at $\sigma = 0$, T_2 decreases to less than half its noise-free value for $\sigma = 2\pi \times 33$ Hz. Our data are in good agreement (within $\pm$ 10%) with the theoretical curve calculated from the resonance lines derived from Eq. (3), with no free parameters. Clearly, as soon as a significant frequency noise is applied, we verify $T_1 \neq T_2$, thus demonstrating the impact of artificially engineered dephasing. This can also be seen as a consequence of the dispersive coupling of the mechanics to fluctuations described by the convolution formalism: the area under the X quadrature resonance curve, which corresponds to the energy stored in the mechanical mode, is preserved

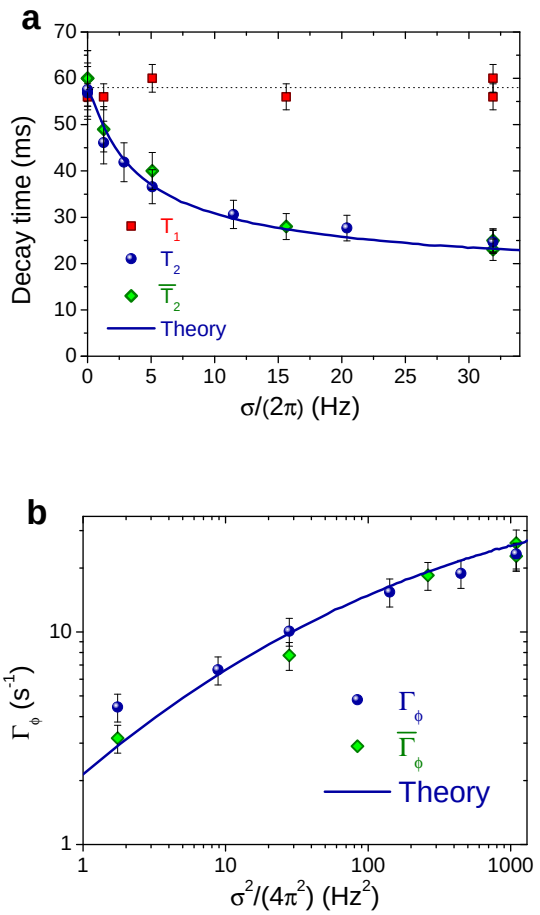

Figure 6: **Controlling pure dephasing. (a)** Measured decay times as a function of injected frequency noise level $\sigma/(2\pi)$. The blue solid line is a theoretical calculation from Eq. (3). Blue dots are obtained from frequency domain measurements, while green dots are obtained from exponential fits of $\langle \mathrm{R} \rangle_N^2$ in time domain measurements. Red dots are time domain measurements of energy relaxation, with the dotted line used as a guide for the eyes. **(b)** Pure dephasing rate as a function of frequency noise level. Blue dots account for frequency domain measurements, green dots represent data from time domain ($\overline{T}_2$) measurements. The blue solid line is the theoretical curve calculated from Eq. (3).

(more mathematical details in supplementary information [28]).

One can then extract the pure dephasing rate $\Gamma_\phi = T_2^{-1} - T_1^{-1}$, as displayed on Fig. 6b). The theoretical curve fits within $\pm$ 15% the data, demonstrating good agreement. This final graph thus presents the relation between Γ_ϕ and $\sigma^2 \propto \int S_\Omega(\omega)\mathrm{d}\omega$, which is the classical mechanical analogue to the superconducting qubit expression which can be found in Ref. [7]. Note that the shape of the curve in Fig. 6b) is also characteristic of the frequency noise probability distribution. The mathematical tools are described thoroughly in supplementary information [28], and can be easily applied as a versatile method describing decoherence even in complicated non-analytic cases like the one presented here.

Discussion

While being a practical quantitative estimate of decoherence, the definition of $T_2 = (\pi W)^{-1}$ or the exponential fit of $\overline{T}_2$ essentially amount to approximating the resonance lineshapes by Lorentzians, which is rather crude. However, defining a shape factor $S = 2\pi W x_{max} / \int \mathrm{Im}[\chi_0(\omega)] F_0 \mathrm{d}\omega$, one can verify how accurate this simple approximation is. For the initial Lorentzian susceptibility we obtain $S = 2/\pi$ as we should. For our strongest level of noise, S only deviates by 20% from this value, which proves that the simple approach is reasonably accurate (see supplementary information [28]).

Obviously, there is information in the measured resonance lineshapes that deserves to be exploited. Highlighting this point is precisely the reason why we created a frequency noise that is non-Gaussian and asymmetric. The complete fits of the lineshapes prove that the theory can handle non-conventional noises. Furthermore, we note that the asymmetry in the resonance is a direct image of the noise properties, as frequency fluctuations here take only positive values. While demanding, the deconvolution of noise from the measured lineshape should be feasible, reconstructing the actual fluctuations distribution. This could prove to be extremely useful in actual experimental systems where dephasing is caused by intrinsic unknown mechanisms. One mathematical technique which has been proposed in the literature is to compute the moments of the frequency response [15], an approach also found in NMR [5].

In summary, we establish that without external influence, pure dephasing is negligible in high quality SiN nanomechanical devices. We measure T_1 and T_2 over an unprecedently large dynamic range, ruling out any possible nonlinear dephasing mechanism, as opposed to carbon-based systems. We then engineer slow fluctuations of the beam's resonance frequency with an external tunable source, unravelling the signatures of pure dephasing. By analogy with quantum bits, we quantita-

tively link the dephasing rate to the characteristic level of noise. We develop the methods that can be applied to a wide range of devices and experiments studying pure dephasing originating from slow frequency fluctuations. Finally, we demonstrate that the lineshapes of the mechanical resonances contain valuable information about the distribution of the frequency fluctuations, and discuss the possibility to extract this information for actual nanomechanical systems suffering from intrinsic sources of noise.

Methods

Device fabrication

The structure was fabricated using e-beam lithography on a silicon substrate covered with a 100 nm silicon nitride (SiN) layer. A 90 nm Aluminum coating has been sputtered onto the sample. It served as a mask for the structure during the Reactive Ion Etching (RIE) step in which SiN has been patterned. The structure was then released using a final XeF_2 etching of the underlying silicon.

Measurements

The voltage drive was delivered with a Tektronix AFG3252 generator, through a 1 kΩ bias resistance. The motion was actuated with the magnetomotive technique, which also leads to the detection of the velocity of the oscillation. In the high Q limit, the velocity in frequency domain is $i\omega_0 x(\omega)$, hence an inverted definition for the signal quadratures X and Y (see supplementary information [28]). The detected signal was processed with a SR 844 RF lock-in amplifier. The output signal was digitized with a 1 Ms/s NI DAQ card (M series PCI-6251). The gate noise voltage was injected with an arbitrary waveform generator Agilent HP34401A, filtered with a low-pass homemade filter, amplified with an EG&G 3113 pre-amplifier (gain of 5000 in amplitude) that also filtered the signal at low frequency.

Data Analysis

The mathematical tools and the theory are described in supplementary information [28] in further details.

References

[1] Armour, A. D., Blencowe, M. P. & Schwab, K. C. Entanglement and Decoherence of a Micromechanical Resonator via Coupling to a Cooper-Pair Box. *Phys. Rev. Lett.* **88**, 148301 (2002).

[2] Remus, L. G., Blencowe, M. P. & Tanaka, Y. Damping and decoherence of a nanomechanical resonator due to a few two-level systems. *Phys. Rev. B* **80**, 174103 (2009).

[3] Cleland, A. N. & Roukes, M. L., Noise processes in nanomechanical resonators. *J. Appl. Phys.* **92**, 2758-2769 (2002).

[4] Unterreithmeier, Q. P., Faust, T. & Kotthaus, J. P. Damping of Nanomechanical Resonators. *Phys. Rev. Lett.* **105**, 027205 (2010).

[5] A. Abragam, *Principles of Nuclear Magnetism*, Oxford University Press (1961).

[6] Schneider, B. H., Singh, V., Venstra, W. J., Meerwaldt H. B. & Steele, G. A. Observation of decoherence in a carbon nanotube mechanical resonator. *Nat. Commun.* **5**, 5819 (2014).

[7] Ithier, G., Collin, E., Joyez, P., Meeson, P. J., Vion, D., Esteve, D., Chiarello, F., Shnirman, A., Makhlin, Y., Schriefl, J. & Schön, G. Decoherence in a superconducting quantum bit circuit. *Phys. Rev. B* **72**, 134519 (2005).

[8] O'Connell, A. D. *et al.* Quantum ground state and single-phonon control of a mechanical resonator. *Nature* **464**, 697-703 (2010).

[9] Faust, T., Rieger, J., Seitner, M. J., Krenn, P., Kotthaus, J. P. & Weig, E. M. Nonadiabatic Dynamics of Two Strongly Coupled Nanomechanical Resonator Modes. *Phys. Rev. Lett.* **109**, 037205 (2012).

[10] Faust, T., Rieger, J., Seitner, M. J., Kotthaus, J. P. & Weig, E. M. Coherent control of a classical nanomechanical two-level system. *Nat. Phys.* **9**, 485-488 (2013).

[11] van Leeuwen, R., Castellanos-Gomez, A., Steele, G. A., van der Zant, H. S. J. & Venstra, W. J. Time-domain response of atomically thin MoS_2 nanomechanical resonators. *Appl. Phys. Lett.* **105**, 041911 (2014).

[12] Eichler, A., Moser, J., Chaste, J., Zdrojek, M., Wilson-Rae, I. & Bachtold, A. Nonlinear damping in mechanical resonators made from carbon nanotubes and graphene. *Nat. Nanotech.* **6**, 339-342 (2011).

[13] Sansa, M., Sage, E., Bullard, E. C., Gély, M., Alava, T., Colinet, E., Naik, A. K., Villanueva, L. G., Duraffourg, L., Roukes, M. L., Jourdan, G. & Hentz S. Frequency fluctuations in silicon nanoresonators. arXiv:1506.08135 [cond-mat.mes-hall] (2015).

[14] Gray, J. M., Bertness, K. A., Sanford, N. A. & Rogers, C. T. Low-frequency noise in gallium nitride nanowire resonators. *Appl. Phys. Lett.* **101** 233115 (2012).

[15] Maizelis, Z. A., Roukes, M. L. & Dykman, M. I. Detecting and characterizing frequency fluctuations of vibrational modes. *Phys. Rev. B* **84** 144301 (2011).

[16] Fong, K. Y., Pernice, W. H. P. & Tang, H. X. Frequency and phase noise of ultrahigh Q silicon nitride nanomechanical resonators. *Phys. Rev. B* **85** 161410 (R) (2012).

[17] Miao, T. F., Yeom, S., Wang, P., Standley, B. & Bockrath, M. Graphene Nanoelectromechanical Systems as Stochastic-Frequency Oscillators. *Nano Lett.* **14**, 2982 (2014).

[18] Zhang, Y., Moser, J., Güttinger, J., Bachtold, A. & Dykman, M. I. Interplay of Driving and Frequency Noise in the Spectra of Vibrational Systems. *Phys. Rev. Lett.* **113**, 255502 (2014).

[19] Eichler, A., Moser, J., Dykman, M. I. & Bachtold, A. Symmetry breaking in a mechanical resonator made from a carbon nanotube. *Nat. Commun.* **4**, 2843 (2013).

[20] Moser, J., Eichler, A., Güttinger, J., Dykman, M. I. & Bachtold, A. Nanotube mechanical resonators with quality factors up to 5 million. *Nat. Nano.* **9**, 1007-1011 (2014).

[21] Gavartin, E., Verlot, P. & Kippenberg, T. J. Stabilization of a linear nanomechanical oscillator to its thermodynamic limit. *Nat. Commun.* **4**, 2860 (2013).

[22] Kleckner, D. *et al.* Creating and verifying a quantum superposition in a micro-optomechanical system. *New J. Phys.* **10**, 095020 (2008).

[23] Verhagen, E., Deléglise, S., Weis, S., Schliesser, A. & Kippenberg, T. J. Quantum-coherent coupling of a mechanical oscillator to an optical cavity mode. *Nature* **482**, 63-67 (2012).

[24] Kozinsky, I., Postma, H. W. Ch., Bargatin I. & Roukes, M. L. Tuning nonlinearity, dynamic range, and frequency of nanomechanical resonators. *Appl. Phys. Lett.* **88**, 253101 (2006).

[25] Collin, E., Defoort, M., Lulla, K., Moutonet, T., Heron, J.-S., Bourgeois O., Bunkov, Yu. M. & Godfrin, H. Insitu comprehensive calibration of a tri-port nano-electromechanical device. *Rev. Sci. Instrum.* **83** (4), 045005 (2012).

[26] Cleland, A. N. & Roukes, M. L. Fabrication of high frequency nanometer scale mechanical resonators from bulk Si crystals. *Appl. Phys. Lett.* **69**, 2653 (1996).

[27] Cleland, A. N. & Roukes, M. L. External control of dissipation in a nanometer-scale radiofrequency mechanical resonator. *Sensors and Actuators* **72** 256 (1999).

[28] Supplementary Information, for detailed calculations and calibrations.

[29] Venstra, W. J., Westra, H. J. R. & van der Zant, H. S. J. Stochastic switching of cantilever motion. *Nat. Commun.* **4**, 2624 (2013).

[30] Mahboob, I., Perrissin, N., Nishiguchi, K., Hatanaka, D. , Y. Okazaki, Fujiwara, A., & Yamaguchi, H., Dispersive and Dissipative Coupling in a Micromechanical Resonator Embedded with a Nanomechanical Resonator, *Nano Lett.* **15**, 2312 (2015).

[31] Nayfeh, A. H. & Mook, D. T. *Nonlinear Oscillations.*, John Wiley & Sons. (1995).

[32] Collin, E., Bunkov, Yu. M. & Godfrin H. Addressing geometric nonlinearities with cantilever microelectromechanical systems: Beyond the Duffing model. *Phys. Rev. B* **82**, 235416 (2010).

Acknowledgements

We thank J. Minet and C. Guttin for help in setting up the experiment, as well as T. Fournier, J.-F. Motte and T. Crozes for help in the device fabrication. We acknowledge support from the ERC CoG grant ULT-NEMS No. 647917, from MICROKELVIN, the EU FRP7 grant No. 228464, and from the French ANR grant QNM No. 0404 01.

Author contributions

All authors contributed to all aspects of the work.

Additional information

Supplementary Information accompanies this paper. **Competing financial interests:** The authors declare no competing financial interests.